Recirculation identified in a 3D alveolar duct reconstructed using synchrotron radiation based X-ray tomographic microscopy

Nenad Filipovic[1,2], David Haberthür[3], Frank S. Henry[1], Danko Milasinovic[2], Dalibor Nikolic[2], Johannes Schittny[3], and Akira Tsuda[1]

[1] Harvard School of Public Health, Boston, [2]University of Kragujevac, Serbia, [3]University of Bern, Switzerland

ABSTRACT

Our previous theoretical analysis, based on a model alveolus with an idealized shape, revealed that the existence (or absence) of rotational flows in the pulmonary alveolus plays a crucial role in the fate of inhaled particles in the pulmonary acinus. To demonstrate that this was not an artifact of the idealized model, we reconstructed parts of an alveolar duct based on synchrotron radiation based X-ray tomographic microscopy (SRXTM). Paraffin embedded and heavy metal stained rat lungs were scanned at the beamline TOMCAT (Swiss Light Source, Paul Scherrer Institut, Switzerland / voxel size = 1.483 um3). After segmentation of the alveolar ducts, straight inlet and outlet sections were added to the 3D reconstruction of a small part of an alveolar duct. The function of the added sections was to straighten the inflow and outflow and to facilitate the imposition of controllable boundary conditions. Finite element grids were generated for the CFD analysis from STL using a 3D cubic algorithm (first, the tetrahedron mesh was created and smoothed, and then transformed into 3D 8-node finite element mesh). Physiological boundary conditions for steady and cyclic flow were imposed at the inlet and outlet of the model. Incompressible fluid motion was described by the 3D Navier-Stokes equations together with the continuity equation and solved numerically with a stabilized finite element method. Pathlines were calculated using the 4th order *Runge-Kutta* method. Due to the large scale of the calculation, the equations were solved on a 40-processor cluster parallel computer.

BACKGROUND

More than a decade ago, we set out to investigate airflow patterns inside the alveolus driven by the motion of expanding and contracting alveolar septal walls (Tsuda et al., 1995), and found that alveolar flow can be highly complex despite the fact that it is typically in a low-Reynolds number viscous flow regime. Similar studies were recently performed by others (Lee & Lee, 2003; Kumar et al., 2009; Darquenne et al., 2009). The most surprising and intriguing implication of this finding is that alveolar flow can be chaotic; that is, it can cause flow-induced mixing (i.e., chaotic mixing), inside the alveoli (Tsuda et al., 1995, 2008a; Haber et al., 2000; Henry et al., 2002, 2009). This discovery was fundamental for the following reasons: 1) it explained theoretically how inhaled aerosol particles can mix with alveolar residual air convectively, rather than diffusively or by any other means attributable to the particles' intrinsic motion, such as inertia-based cross-streamline; 2) it implied that in any alveolus with rotational flow can generate chaotic convective mixing (Fig. 1).

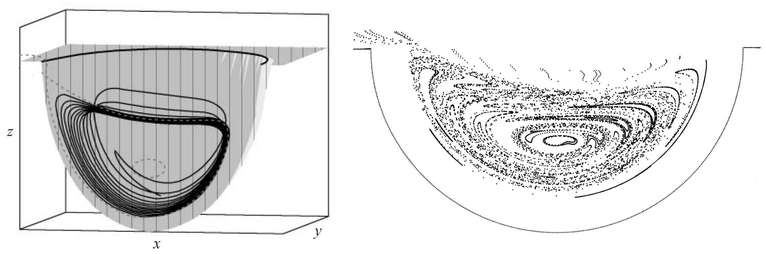

Fig. 1 3-dimensional spherical alveolus model with rhythmically expanding walls. *Left*: a typical streamline escaping from (or converging to) the stagnation saddle point on the symmetry plane, pointing outward toward the alveolus boundaries during inhalation, and toward stagnation during exhalation. *Right*: a Poincare map for points initially placed on the symmetry plane. (Haber et al., 2000).

OBJECTIVES

Previous theoretical/computational analyses, which showed the existence (or absence) of rotational flows in the pulmonary alveolus, are all based on a model alveolus with an idealized shape. The aim of this project is to demonstrate that rotational flows are not an artifact of the idealized model.

METHODS

The geometry of an alveolar duct of an adult rat was reconstructed based on data obtained by synchrotron radiation based X-ray tomographic microscopy (SRXTM). Fig.2 shows a workflow chart of our Finite element-based 3D reconstruction analysis. Paraffin embedded and heavy metal stained rat lungs were scanned at the beamline TOMCAT (Swiss Light Source, Fig. 3) and a stack of 2D raw images was made with the resolution of 1.4um/pixel (Fig. 4).

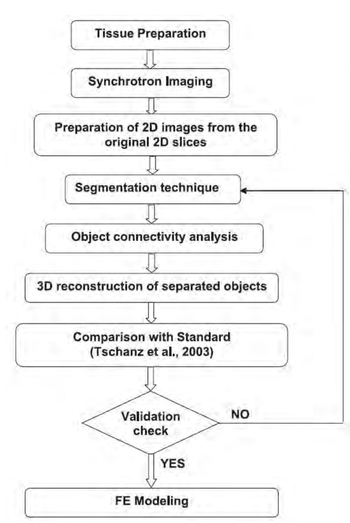

Fig. 2 (*left*) Workflow diagram outlining protocol for high-resolution 3-dimensional (3D) reconstruction of the acinus.

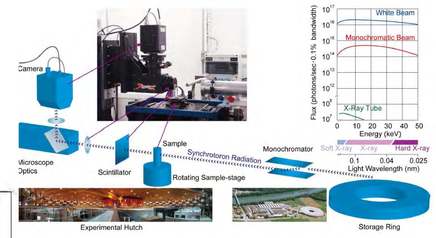

Fig. 3 (*above*) Imaging setup. The X-rays are coupled out of the storage ring via a wiggler. The monochromator is then used to select a desired wavelength of the incident X-rays. The sample is placed on a rotating sample holder inside the beam. While the X-rays penetrate the sample, the stage is rotated, and in total 1,500 projections over 180 degrees are recorded. Plot shows spectrum of TOMCAT (red and blue) compared with conventional X-ray tube (green).

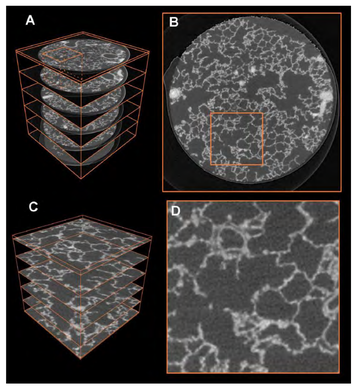

Fig. 4 (above) Overview of workflow for the selection of a region of interest (ROI). *A*: full perspective view of a rat lung sample with 6 selected orthogonal slices and bounding box of the full sample in orange. The ROI selected for subfigures *C* and *D* is visible in the *top left*. *B*: close-up of one slice of the full dataset with selected ROI (sidelength of 256 pixels). *C*: ROI cut out of the full sample, 6 selected orthogonal slices are shown. *D*: close-up of the ROI in subfigure (*B*).

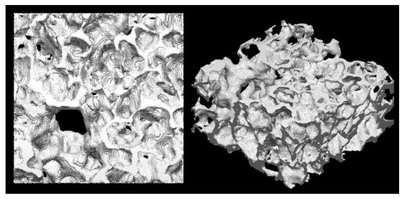

Fig. 5 (above) 3-dimensional reconstruction of rat lung tissue (Tsuda et al., 2008b).

Geometric model: After segmentation of the alveolar ducts, straight inlet and outlet sections were added to the 3D reconstruction of a small part of an alveolar duct. The function of the added sections was to straighten the inflow and outflow and to facilitate the imposition of controllable boundary conditions. Finite element (FE) grids were generated from STL using a 3D cubic algorithm (first, a tetrahedron mesh was created and smoothed, and then transformed into 3D 8-node finite element mesh) (Fig. 6).

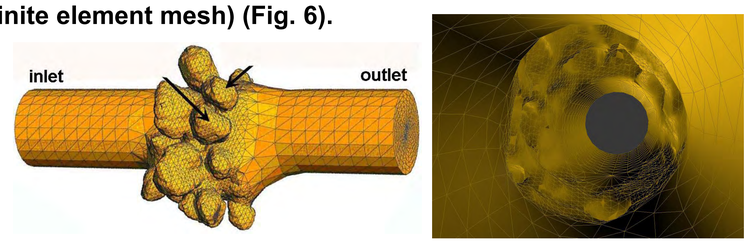

Fig. 6 Geometric model of rat alveolar duct. Left: Outside view, Right: Inner view.

Computational Fluid Dynamics (CFD): Physiological boundary conditions for steady and cyclic flow were imposed at the inlet and outlet of the model. Incompressible fluid motion was described by the 3D Navier-Stokes equations together with the continuity equation and solved numerically with a stabilized FE method. Pathlines were calculated using the 4th order *Runge-Kutta* method. Due to the large scale of the calculation, the equations were solved on a 40-processor cluster parallel computer.

RESULTS

The predicted streamline patterns in 3D reconstructed alveoli exhibit alveolar recirculation flows of many different sizes and shapes (Fig. 7), consistent with the findings of our experimental investigations (Fig. 8).

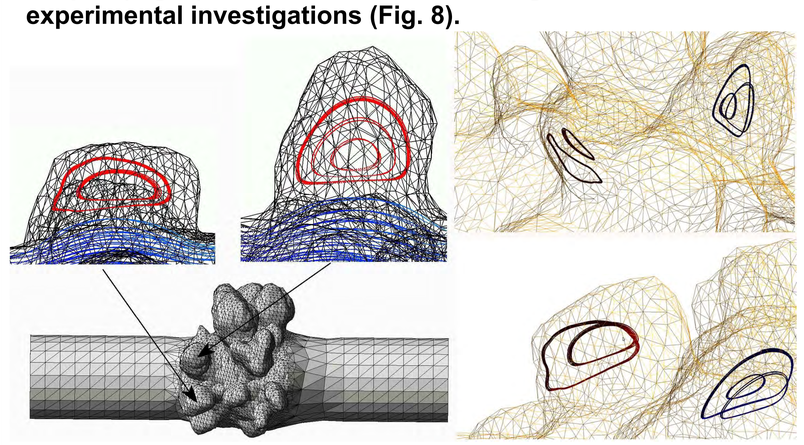

Fig. 7 Steady airflow at a Reynolds number of 0.4 (determined by the inlet duct diameter and mean ductal velocity).

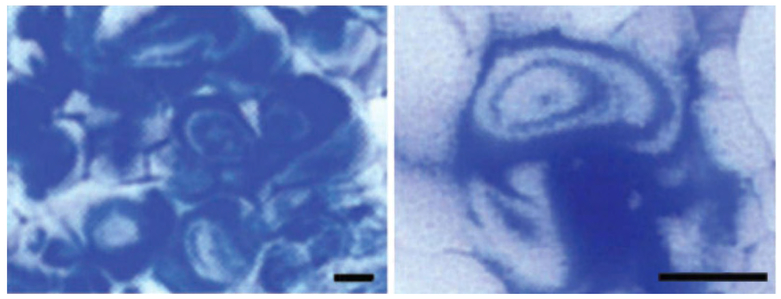

Fig. 8 Experimental evidence of recirculation flow within alveoli. (Tsuda et al., 2002)

CONCLUSIONS

Our CFD analysis demonstrates and confirms that rotational flows can be generated inside the 3D reconstructed alveoli if they are sufficiently deep.

This work was supported in part by NIH HL070542, HL074022, HL054885, Swiss National Science Foundation 3100A0-109874 + 310030-125397

REFERENCES

Darquenne *et al*. *Phil. Trans. R. Soc. A* 367: 2333-2346, 2009.

Haber *et al*. *J. Fluid Mech.* 405: 243-268, 2000.

Henry *et al*. *J. Appl. Physiol.* 92:835-845, 2002.

Henry *et al*. *ASME J. Biomech. Eng.* 131(1):011006, 2009.

Kumar *et al*. *J Biomech.* 42(11):1635-42, 2009.

Lee & Lee. *J Aero Sci*. 34: 1193-1215, 2003.

Tsuda *et al*. *J. Appl. Physiol.* 79:1055-1063, 1995.

Tsuda *et al*. *J. Appl. Physiol.* 105:964–976, 2008a.

Tsuda *et al*. *Respir. Physiol. Neurobiol.* 163(1-3):139-49, 2008b.